IMPACT OF ANISOTROPIC PERMEABILITY ON MICROPOLAR FLUID DYNAMICS AND HEAT TRANSFER IN POROUS CHANNELS

R. Vijaya Sree[a, b], **V. K. Narla**[b*]

aACE Engineering College, Ghatkesar Mandal, Medchal District, Telangana, 501301, India
bGITAM Deemed to be University, Department of Mathematics, Hyderabad, 502329, India
∗Corresponding Author e-mail: vnarla@gitam.edu

The current study explores the fluid dynamics and heat transfer characteristics of micropolar fluids within a channel filled with anisotropic porous media. The governing equations for the fluid flow, microrotation, and temperature profiles are numerically solved using Spectral Quasi-Linearization Method (SQLM). The research examines the influence of various key parameters such as the anisotropic permeability ratio, anisotropic angle, Darcy number, Reynolds number, Brinkman number, Prandtl number, and coupling number. Key findings indicate that the anisotropic permeability ratio and anisotropic angle significantly affect fluid flow and heat distribution, with increased anisotropy leading to enhanced microrotation and temperature, albeit with reduced velocity at the channel center. Higher Darcy numbers result in less restricted flow, increasing velocity and reducing microrotation effects, while increasing the coupling number contributes to a more uniform temperature profile. These results provide significant insights into the optimization of heat transfer and flow control in engineering applications that involve micropolar fluids in porous media.

Keywords: *Micropolar fluid; Anisotropic porous media; Anisotropic permeability; Microrotation; Heat transfer; Spectral Quasi-Linearization method*

PACS: 47.50.-d; 47.56.+r; 44.30.+v; 44.15.+a; 02.70.Hm

1. INTRODUCTION

The advent of the micropolar fluid theory occurred in recent decades due to the necessity to model a fluid with rotating micro-components. Micropolar fluids are fluids that display a correlation between the rotational dynamics of particles and the overall velocity structure at a large scale. Suspension of hard particles in a viscous medium forms these fluids. Liquid Crystals, magnetic fluids(ferrofluids), blood, and lubricants with additives are examples of micropolar fluids. Other industrial applications, including biological structures, lubricant fluids, and polymer solutions, utilise micropolar fluids. Micropolar fluids theory has been extensively investigated by researchers worldwide. Eringen [1] revolutionised the micropolar fluid framework and polymer solutions which make use of these fluids. He derived the micropolar fluid flow governing equations and boundary conditions and implemented them in analysis of channel flow, taking into account the thermodynamic limitations. Researchers have investigated the kinetics of both natural and combined convection flows of micropolar fluids on flat and cylindrical surfaces [2]–[5]. Mirzaaghaian et al. [6] analysed the flow characteristics of a micropolar fluid and the dynamics of heat transfer in a porous conduit. To solve nonlinear equations the Differential Transformation Method (DTM) [7]–[11] was utilised. In this study, the influencing factors were the Peclet number, Reynolds number, and the micro-rotation/angular velocity. The findings showed that while the temperature and concentration fields will only slightly alter, the stream function will be greatly altered by varying the Reynolds number. An analysis was conducted by Mabood et al. [12] to investigate the flow and heat transfer properties of a micropolar fluid across a stretchable sheet in a porous media. The flow was exposed to a magnetic field, thermodiffusion, and variable heat sources in their work and solutions were obtained for the resultant equations. A comparison of outcomes with earlier research revealed very good agreement. The research revealed that the distribution of velocity decreased as the parameter for the magnetic field increased, despite the fact that the thermal and concentration distribution were elevated.

Extensive research conducted globally on the use of micropolar and nanofluid fluids has shown promising results for various industrial processes and scientific research oriented applications, including heat exchangers, combined propulsion systems, and medical procedures. Many researchers [13]–[18] have conducted an in-depth review of the fundamental principles governing micropolar fluid flow in porous conduits. The behaviour of micropolar fluid in a conduit confined by two parallel permeable walls was analysed by Jalili et al. [19]. The fluid flow was considered two-dimensional, and steady. It was observed that with the exception of the dimensionless microrotation profile, all of the mentioned dimensionless parameters have increasing average values when the values of coupling number increase. Moreover, temperature distribution is the most significant parameter that can be affected by Peclet number for heat diffusion. The solution for this problem shows that the averages of the dimensionless parameters reduce if the ratio of micropolar-inertia density is increased along channel, with the exception of the non-dimensional flow function characteristics. Under the presumptions of heat radiation and reaction rate coefficients, Shamshuddin et al. [20] analysed the dynamics of a micropolar

---

fluid flow through a conduit considering both combined and non-linear heat transfer. It was shown how the temperature, concentration, and dimensionless velocity of micropolar fluid reached their peak values near the channel's centre. The dynamics of mass and heat tranfer in micropolar fluids are determined by their thermal and solution properties.

Abdalbagi [21] examined the dynamics of a micropolar fluid flow and characteristics of heat transfer in a porous conduit, applying the method of iterative linearization. This study showed that fluid flow, mass transport, microrotation and heat transfer are all positively impacted by increasing coupling and spin-gradient viscosity parameters. Conversely, these profiles exhibit a decline as micro-inertia density increases. While an increased Peclet number indicates optimised heat transfer by convection and mass transfer, higher Reynolds numbers reduce the distributions of velocity, microrotation, and temperature. Micropolar fluid framework, which is applicable to non-Newtonian fluids, accounts for microrotation and also couple stresses. The research explores how the magnetic force field slows down the flow of fluid, while channel permeability increases velocity. Heat radiation enhances the temperature distribution, impacting heat transfer. The findings have practical significance in the domains of engineering like temperature control systems, and MHD generators, where these conditions are frequently encountered. A study by Shah et al. [22] provided a description of the fluid flow dynamics and heat transfer of blood-infused gold micropolar nanofluids in a porous conduit. The channel contained thermal radiation whether the walls were in motion or rest. Blood was considered as the base fluid, and microgold was thought to be the polar nanofluid. The study conducted by Ahmad et al. [23] investigated the problem of mass and heat transfer in a micropolar fluid flow within a porous conduit using a Quasi-linearization approach. At fluid temperatures above a certain threshold, the concurrent phenomena of heat radiation buildup, absorption heat, heat exchange, and Brownian flow were observed. When it comes to magnetic parameters and materials, supportive engineering forces like velocity, skin friction, and heat exchange have proven to be beneficial. However, the transfer rate of mass showed an opposite response. Akbarzadeh et al. [24] analysed the flow of a nanofluid which was considered laminar and forced convective heat transport within a wavy channel. In their study, it was demonstrated that if the aspect ratio of the conduit is increased, the average Nusselt number becomes more sensitive to the Reynolds number and also to the aspect ratio of the channel. The gradient of the temperature on the left sheet will decrease as the motion parameter increases. However, the gradient exhibits a positive correlation with Lorentz forces. The effects of thermal radiation and also thermo-diffusion on Williamson model nanofluid along a porous and stretchable surface were examined by Rashidi, and Bhatti [25]. Their findings showed that the fluid's magnitude increases with large porosity and Williamson fluid parameters. On the other hand, the gradient on the left sheet increases as Lorentz forces do. In a transverse magnetic force field presence, Rashidi et al. [26] examined the exchange of heat for a nanofluid flow along a stretchable sheet while considering buoyancy effects, and heat radiation into account. It has been noticed that nanofluid's velocity rises when the buoyancy factor is increased while the distribution of temperature decreases. Assuming the fluid is incompressible and steady, Takhar et al. [27] analysed the problem of axisymmetric flow of micropolar fluid and heat transfer between two permeable discs. A finite analysis method was employed to solve the flow governing equations, which describes the velocity, temperature and also microrotation. Quantitative simulations have been conducted to determine the axial, radial, microrotation velocities, temperature, couple stress coefficient, skin friction, and heat transfer rate on the discs, for varying values of injection Reynolds number and micropolar parameter.

The empirical study conducted by Pathak et al. [28] examined the flow and heat transfer properties of micropolar fluids along a stretchable sheet in a Darcy porous media. The flow governing system of equations, which are nonlinear, were solved by the authors using a quasi-uniform mesh in conjunction with a nonstandard finite difference approach. Validation of the results was achieved by a comparison with those computed using the RK method of order four. The results indicate that the boundary layer thickness was reduced with an increase in the values of the Reynolds number, micropolar parameter, and injection/suction parameter. Additionally, a rise in the Prandtl number, heat index parameter, and the micropolar and injection/suction parameters enhances microrotation, indicating a more pronounced effect of the micropolar characteristics on the dynamics of fluid flow and heat transfer. In their study, Cutis [29] examined the phenomenon of a creeping flow in an incompressible, micropolar fluid bounded over a permeable shell. Empirical evidence demonstrated that when hydraulic resistivity is low and the sphere is completely porous, efficient circulation occurs between the porous area and the surrounding fluid. This finding can be utilised for efficient drug delivery by using a fully porous sphere with outstanding permeability as the carrier for the drug.

Recent progress has centered on creating effective numerical techniques to address the complex, nonlinear differential equations that control fluid flow dynamics. The Spectral Quasi-Linearization Method (SQLM) is one such technique, combining quasilinearization with spectral methods to achieve high accuracy in linearizing and solving nonlinear terms. This method is effectively used for investigating boundary layer flows over stretching/shrinking sheets in non-Darcy porous media and other fluid flow applications. Srinivasacharya et al. [30] have examined the process of production of entropy and heat exchange in a micro-polar fluid flow inside an annular region subjected to a magnetic field. The two geometry walls in this study, one acting as suction and the other as injection, have the same velocity. The solution was obtained using a spectral Chebyshev collocation method. These findings demonstrate that the interior cylinder exhibited the greatest entropy production, whereas the exterior cylinder displayed the lowest entropy production. Alharbey et al. [31] employed Structural Equation Modelling (SQLM) to investigate the dynamics of a micropolar fluid along a horizontal plate within a non-Darcy porous media. Similarity variables in SQLM convert flow-governing equations into ODE, resulting in numerical solutions with rapid convergence. Entropy production decreases with Reynolds and Brinkman numbers, while velocity profiles increase with material parameters, demonstrating the method's resilience and effectiveness in complex fluid dynamics applications.

Majority of the studies reported in the literature focused on the study of micropolar fluid flow with regard to stretching sheets or within porous conduits. This work presents a mathematical model for the analysis of flow and heat transfer phenomena in a micropolar fluid in between a channel with parallel and permeable walls, saturated with anisotropic porous media. The momentum and energy equations, together with the boundary conditions, are initially transformed into a non-dimensional form by similarity transformation. Subsequently, a numerical solution is obtained using the Spectral Quasi-Linearization Method (SQLM). A systematic investigation is conducted to examine the influence of several key parameters, including the anisotropic permeability ratio, anisotropic angle, Darcy number, Reynolds number, Brinkmann number, Prandtl number, and coupling number on the velocity, microrotation, and temperature distributions within the boundary layer.

2. MATHEMATICAL FORMULATION OF THE PROBLEM

Consider a 2-D channel filled with anisotropic porous media, where the flow of a steady, laminar, incompressible micropolar fluid is observed. This work assumes that the channel walls are permeable, enabling the steady flow of fluid into or out of the channel at a constant velocity of v_0. The X-axis is aligned parallel to the surface of the channel walls, while the Y-axis exhibits a perpendicular orientation to them. Moreover, the channel walls are situated at $y = \pm h$ and the temperatures near the boundaries are represented as T_1 and T_2, respectively (see Figure 1). As the porous media is considered anisotropic the permeability matrix which is a second-order tensor $\mathbb{K}$, is given by [32]

$$\mathbb{K} = \begin{bmatrix} k_2 \cos^2 \phi + k_1 \sin^2 \phi & (k_2 - k_1) \sin \phi \cos \phi \\ (k_2 - k_1) \sin \phi \cos \phi & k_2 \sin^2 \phi + k_1 \cos^2 \phi \end{bmatrix}. \tag{1}$$

k_1 and k_2 are the vertical and horizontal permeabilities which are assumed constant. ϕ is the anisotropic angle formed by the intersection of the main axis and the horizontal permeability k_2. The governing equations for micropolar fluid with
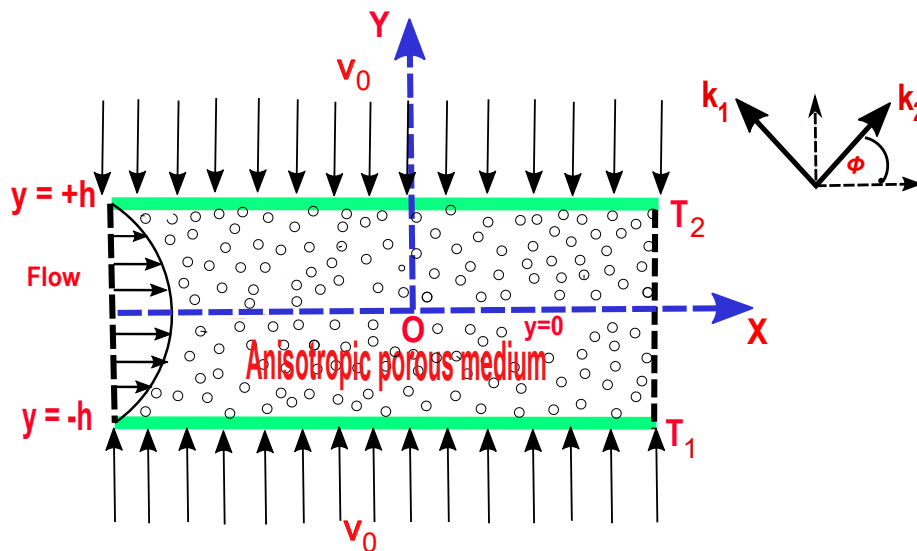

Figure 1. A physical interpretation of micropolar fluid flow problem.

anisotropic porous permeability are stated below, taking into account the aforementioned factors:

$$\frac{\partial u}{\partial x} + \frac{\partial v}{\partial y} = 0, \tag{2}$$

$$\rho \left[u \frac{\partial u}{\partial x} + v \frac{\partial u}{\partial y} \right] = -\frac{\partial p}{\partial x} + (\mu + \kappa) \left[\frac{\partial^2 u}{\partial x^2} + \frac{\partial^2 u}{\partial y^2} \right] + \kappa \frac{\partial W}{\partial y}$$
$$- \frac{\mu + \kappa}{k_1 k_2} \left[(k_1 \cos^2(\phi) + k_2 \sin^2(\phi))u + (\frac{1}{2}(k_1 - k_2) \sin(2\phi))v \right], \tag{3}$$

$$\rho \left[u \frac{\partial v}{\partial x} + v \frac{\partial v}{\partial y} \right] = -\frac{\partial p}{\partial y} + (\mu + \kappa) \left[\frac{\partial^2 v}{\partial x^2} + \frac{\partial^2 v}{\partial y^2} \right] - \kappa \frac{\partial W}{\partial x}$$
$$- \frac{\mu + \kappa}{k_1 k_2} \left[(\frac{1}{2}(k_1 - k_2) \sin 2(\phi))u + (k_1 \sin^2(\phi) + k_2 \cos^2(\phi))v \right], \tag{4}$$

$$\rho j \left[u \frac{\partial W}{\partial x} + v \frac{\partial W}{\partial y} \right] = -\kappa \left[2W + \frac{\partial u}{\partial y} - \frac{\partial v}{\partial x} \right] + \gamma \left[\frac{\partial^2 W}{\partial x^2} + \frac{\partial^2 W}{\partial y^2} \right], \tag{5}$$

$$(\rho c_p) \left[u \frac{\partial T}{\partial x} + v \frac{\partial T}{\partial y} \right] = K_f \left[\frac{\partial^2 T}{\partial x^2} + \frac{\partial^2 T}{\partial y^2} \right] + \frac{\kappa}{2} \left[\frac{\partial v}{\partial x} - \frac{\partial u}{\partial y} - 2W \right]^2 + \gamma \left[\left(\frac{\partial W}{\partial x} \right)^2 + \left(\frac{\partial W}{\partial y} \right)^2 \right]$$
$$+ (2\mu + \kappa) \left[(\frac{\partial u}{\partial x})^2 + (\frac{\partial v}{\partial y})^2 + \frac{1}{2} (\frac{\partial u}{\partial y} + \frac{\partial v}{\partial x})^2 \right] \tag{6}$$
$$+ \frac{\mu + \kappa}{k_1 k_2} \left[(k_1 \cos^2(\phi) + k_2 \sin^2(\phi)) u^2 + (k_1 - k_2) \sin 2(\phi) uv + (k_2 \cos^2(\phi) + k_1 \sin^2(\phi)) v^2 \right].$$

Mathematical formulations for boundary conditions of a micropolar fluid flow problem are as below:

$$u = 0, \ v = -v_0, \ W = 0, \ T = T_1, \ \text{at} \ y = -h,$$
$$u = 0, \ v = v_0, \ W = 0, \ T = T_2, \ \text{at} \ y = +h. \tag{7}$$

The variables u and v in the equations above represent the dimensional components of fluid velocity in X and Y coordinate directions. Furthermore, the variables considered are: p denotes pressure, T denotes temperature, W denotes microrotation velocity, κ denotes vortex viscosity, γ denotes spin-gradient viscosity, j denotes micro-inertia density, ρ denotes the effective density of the micropolar fluid, μ denotes effective dynamic viscosity of micropolar fluid, c_p denotes specific heat of micropolar fluid, and K_f denotes the thermal conductivity of micropolar fluid.
Following dimensionless parameters are introduced:

$$\xi = \frac{x}{h}, \ \eta = \frac{y}{h}, \ u = -\frac{v_0 x}{h} f'(\eta), \ W = \frac{v_0 x}{h^2} g(\eta), \ v = v_0 f(\eta), \ \theta = \frac{(T - T_1)}{(T_2 - T_1)} = \theta_1(\eta) + \xi^2 \theta_2(\eta). \tag{8}$$

In these equations, v_0 is the cross-flow transpiration velocity, which remains constant. $v_0 < 0$ stands for suction and $v_0 > 0$ for injection. After substituting the above into the flow governing equations (3)- (6) and after the pressure gradient is removed, and upon equating the coefficients of ξ^0, ξ, and ξ^2 we get:

$$\left(\frac{1}{1 - N} \right) f^{iv} - \frac{N}{1 - N} g'' + Re[f' f'' - f f'''] - \frac{1}{(1 - N)Da} [K \cos^2 \phi + \sin^2 \phi] f'' = 0, \tag{9}$$

$$\left(\frac{2 - N}{m^2} \right) g'' - 2g + Re \, a_j \left(\frac{1 - N}{N} \right) (f'g - fg') + f'' = 0, \tag{10}$$

$$\theta_1'' + 2\theta_2 - Pr \, Re[f\theta_1'] + \frac{N(2 - N)}{1 - N} \frac{Br}{m^2} g^2 + \frac{Br}{Da} [\cos^2 \phi + K \sin^2 \phi] f^2$$
$$+ 2\left(\frac{2 - N}{1 - N} \right) Br f'^2 = 0, \tag{11}$$

$$\theta_2'' + \frac{Br}{2} \left(\frac{N}{1 - N} \right) [f''^2 + 4g^2 - 4f''g] + \frac{Br}{m^2} g'^2 \left(\frac{N(2 - N)}{1 - N} \right) + 2Pr \, Re \, \theta_2 f' - Pr \, Re f \theta_2'$$
$$+ \frac{Br}{2} \left(\frac{2 - N}{1 - N} \right) f''^2 + \frac{Br}{(1 - N)Da} [K \cos^2 \phi + \sin^2 \phi] f'^2 = 0. \tag{12}$$

The boundary conditions are:

$$f(\eta) = -1, \ f'(\eta) = 0, \ g(\eta) = 0, \ \theta_1(\eta) = 0, \ \theta_2(\eta) = 0 \ \text{at} \ \eta = -1,$$
$$f(\eta) = 1, \ f'(\eta) = 0, \ g(\eta) = 0, \ \theta_1(\eta) = 1, \ \theta_2(\eta) = 0, \ \text{at} \ \eta = 1. \tag{13}$$

Here Br represents Brinkman number, Pr represents Prandtl number, Re represents Reynolds number, Da represents Darcy number, N represents coupling number, a_j represents micro-inertia parameter, m^2 represents micropolar parameter, K represents anisotropic permeability ratio. These parameters are defined as below:

$$Br = \frac{\mu v_0^2}{K_f(T_2 - T_1)}, \ Pr = \frac{\mu c_p}{K_f}, \ Re = \frac{\rho v_0 h}{\mu}, \ Da = \frac{k_1}{h^2},$$
$$N = \frac{\kappa}{(\kappa + \mu)}, \ a_j = \frac{j}{h^2}, \ m^2 = \frac{(\kappa + 2\mu)h^2 \kappa}{(\kappa + \mu)\gamma}, \ K = \frac{k_1}{k_2}. \tag{14}$$

3. METHOD OF SOLUTION

A numerical solution was obtained for the non-linear equations (9) - (12) by applying the Spectral Quasi-Linearization approach, while considering the boundary conditions in equation (13). This iterative approach combines a spectral framework with a Quasi-linearization method for solving nonlinear differential equations. Bellman and Kalaba [33] developed the Quasilinearization Method (QLM) as an extension of the Newton-Raphson method, specifically designed to address nonlinear boundary value problems. On applying the above procedure, the linear equations are obtained as:

$$e_{1,r} f^{iv}_{r+1} + e_{2,r} f'''_{r+1} + e_{3,r} f''_{r+1} + e_{4,r} f'_{r+1} + e_{5,r} f_{r+1} + e_{6,r} g''_{r+1} = S_1, \tag{15}$$

$$f''_{r+1} + e_{7,r} f'_{r+1} + e_{8,r} f_{r+1} + e_{9,r} g''_{r+1} + e_{10,r} g'_{r+1} + e_{11,r} g_{r+1} = S_2, \tag{16}$$

$$e_{12,r} f'_{r+1} + e_{13,r} f_{r+1} + e_{14,r} g_{r+1} + (\theta_1)''_{r+1} + e_{15,r} (\theta_1)'_{r+1} + e_{16,r} (\theta_2)_{r+1} = S_3, \tag{17}$$

$$e_{17,r} f''_{r+1} + e_{18,r} f'_{r+1} + e_{19,r} f_{r+1} + e_{20,r} g'_{r+1} + e_{21,r} g_{r+1} + (\theta_2)''_{r+1} + e_{22,r} (\theta_2)'_{r+1} + e_{23,r} (\theta_2)_{r+1} = S_4. \tag{18}$$

The obtained boundary conditions are :

$$\begin{aligned} f_{r+1} = -1, \ f'_{r+1} = 0, \ g_{r+1} = 0, \ (\theta_1)_{r+1} = 0, \ (\theta_2)_{r+1} = 0 \ \text{at} \ \eta = -1, \\ f_{r+1} = 1, \ f'_{r+1} = 0, \ g_{r+1} = 0, (\theta_1)_{r+1} = 1, \ (\theta_2)_{r+1} = 0, \ \text{at} \ \eta = 1. \end{aligned} \tag{19}$$

The coefficients obtained are as follows:

$$\mathrm{e}_{1,r} = \frac{1}{1-N}, \quad e_{2,r} = -Re f_r, \quad e_{3,r} = -\frac{1}{(1-N)Da}[K\cos^2\phi + \sin^2\phi] + Re f'_r, \quad e_{4,r} = Re f''_r,$$

$$e_{5,r} = -Re f'''_r, \quad e_{6,r} = -\frac{N}{1-N}, \quad e_{7,r} = Re\, a_j(\frac{1-N}{N})g_r, \quad e_{8,r} = -Re\, a_j(\frac{1-N}{N})g'_r, \quad e_{9,r} = \frac{2-N}{m^2},$$

$$e_{10,r} = -Re\, a_j(\frac{1-N}{N})f_r, \quad e_{11,r} = Re\, a_j(\frac{1-N}{N})f'_r - 2, \quad e_{12,r} = 4(\frac{2-N}{1-N})Br\, f'_r,$$

$$e_{13,r} = -Pr\, Re(\theta'_1)_r + 2\frac{Br}{(1-N)Da}[\cos^2\phi + K\sin^2\phi]\, f_r, \quad e_{14,r} = \frac{2N(2-N)}{1-N}\frac{Br}{m^2}\, g_r, \quad e_{15,r} = -Pr Re f_r,$$

$$e_{16,r} = 2, \quad e_{17,r} = \frac{N}{1-N}Br(f'')_r - \frac{2N}{1-N}Br\, g_r + \frac{2-N}{1-N}Br(f'_r),$$

$$e_{18,r} = 2Pr\, Re(\theta_2)_r + \frac{2Br}{(1-N)Da}[K\cos^2\phi + \sin^2\phi]f'_r, \quad e_{19,r} = -PrRe(\theta'_2)_r, \quad e_{20,r} = \frac{2N(2-N)}{1-N}\frac{Br}{m^2}g'_r,$$

$$e_{21,r} = \frac{4N}{1-N}Br\, g_r - \frac{2N}{1-N}Br(f'')_r, \quad e_{22,r} = -Pr\, Re f_r, \quad e_{23,r} = 2Pr\, Re f'_r,$$

$$S_1 = Re[f'_r f''_r - f_r f'''_r], \quad S_2 = Re\, a_j(\frac{1-N}{N})[f'_r g_r - f_r g'_r],$$

$$S_3 = -Pr\, Re(f)_r(\theta'_1)_r + \frac{N(2-N)}{1-N}\frac{Br}{m^2}(g)_r^2 + \frac{Br}{(1-N)Da}[\cos^2\phi + K\sin^2\phi](f)_r^2 + \frac{2(2-N)}{1-N}Br(f')_r^2,$$

$$S_4 = \frac{1}{2}(\frac{N}{1-N})Br[(f'')_r^2 + 4(g)_r^2 - 4(f'')_r g_r] + \frac{N(2-N)}{1-N}\frac{Br}{m^2}(g')_r^2 + 2PrRe(f')_r - PrRe(f)_r(\theta'_2)_r$$

$$+ \frac{1}{2}(\frac{2-N}{1-N})Br(f''^2)_r + \frac{Br}{(1-N)Da}[K\cos^2\phi + \sin^2\phi](f')_r^2.$$

To solve the linearised equations (15)-(18), a Chebyshev spectral collocation approach [34, 35] is used. Chebyshev interpolating polynomials are used to estimate the unknown functions. These polynomials are collocated at the Gauss-Lobatto points, which are defined as $\zeta_j = \cos(\pi j/M)$, where $j = 1, 2, \cdots M$ of collocation points. The derivatives of $f(\eta)$, $g(\eta)$, $\theta_1(\eta)$, and $\theta_2(\eta)$ are determined by using the differential matrix **D** to calculate Chebyshev polynomials from the collocation nodes. At the collocation nodes, the derivatives of f_{r+1}, g_{r+1}, $(\theta_1)_{r+1}$, and $(\theta_2)_{r+1}$ are represented as:

$$\frac{\partial^P f_{r+1}}{\partial \eta^P} = \left(\frac{2}{L}\right)^P \sum_{i=0}^{M} D^p_{M,i} f_{r+1}(\eta_i) = \mathbf{D}^P F,$$

$$\frac{\partial^P g_{r+1}}{\partial \eta^P} = \left(\frac{2}{L}\right)^P \sum_{i=0}^{M} D^p_{M,i} g_{r+1}(\eta_i) = \mathbf{D}^P G,$$

$$\frac{\partial^P (\theta_1)_{r+1}}{\partial \eta^P} = \left(\frac{2}{L}\right)^P \sum_{i=0}^{M} D^p_{M,i} (\theta_1)_{r+1}(\eta_i) = \mathbf{D}^P \Theta_1,$$

$$\frac{\partial^P (\theta_2)_{r+1}}{\partial \eta^P} = \left(\frac{2}{L}\right)^P \sum_{i=0}^{M} D^p_{M,i} (\theta_2)_{r+1}(\eta_i) = \mathbf{D}^P \Theta_2.$$

(20)

Where **D** is Chebyshev differentiation matrix which is scaled by $L/2$ and is of order $(M+1) \times (M+1)$ with derivative of order p. On substituting the equation (20) into equations (15) - (18), we obtain

$$[e_{1,r}\mathbf{D}^4 + e_{2,r}\mathbf{D}^3 + e_{3,r}\mathbf{D}^2 + e_{4,r}\mathbf{D} + e_{5,r}I]f_{r+1} + e_{6,r}\mathbf{D}^2 g_{r+1} = S_1, \tag{21}$$

$$[\mathbf{D}^2 + e_{7,r}\mathbf{D} + e_{8,r}I]f_{r+1} + [e_{9,r}\mathbf{D}^2 + e_{10,r}\mathbf{D} + e_{11,r}I]g_{r+1} = S_2, \tag{22}$$

$$[e_{12,r}\mathbf{D} + e_{13,r}I]f_{r+1} + [e_{14,r}I]g_{r+1} + [\mathbf{D}^2 + e_{15,r}\mathbf{D}](\theta_1)_{r+1} + [e_{16,r}I](\theta_2)_{r+1} = S_3, \tag{23}$$

$$[e_{17,r}\mathbf{D}^2 + e_{18,r}\mathbf{D} + e_{19,r}I]f_{r+1} + [e_{20,r}\mathbf{D} + e_{21,r}I]g_{r+1} + [\mathbf{D}^2 + e_{22,r}\mathbf{D} + e_{23,r}I](\theta_2)_{r+1} = S_4. \tag{24}$$

On applying the spectral method to boundary conditions we get:

$$f_{r+1}(\zeta_0) = 1, \quad \sum_{k=0}^{M} \mathbf{D}_{M,k} f_{r+1}(\zeta_0) = 0,$$

$$f_{r+1}(\zeta_M) = -1, \quad \sum_{k=0}^{M} \mathbf{D}_{M,k} f_{r+1}(\zeta_M) = 0,$$

$$g_{r+1}(\xi_0) = 0, \quad g_{r+1}(\zeta_M) = 0, \tag{25}$$

$$(\theta_1)_{r+1}(\zeta_0) = 1, \quad (\theta_1)_{r+1}(\zeta_M) = 0,$$

$$(\theta_2)_{r+1}(\zeta_0) = 0, (\theta_2)_{r+1}(\zeta_M) = 0.$$

The matrix form of the aforementioned equation system is written as

$$\begin{bmatrix} \mathbf{A}_{11} & \mathbf{A}_{12} & \mathbf{A}_{13} & \mathbf{A}_{14} \\ \mathbf{A}_{21} & \mathbf{A}_{22} & \mathbf{A}_{23} & \mathbf{A}_{24} \\ \mathbf{A}_{31} & \mathbf{A}_{32} & \mathbf{A}_{33} & \mathbf{A}_{34} \\ \mathbf{A}_{41} & \mathbf{A}_{42} & \mathbf{A}_{43} & \mathbf{A}_{44} \end{bmatrix} \times \begin{bmatrix} F_{r+1} \\ G_{r+1} \\ \Theta_{1r+1} \\ \Theta_{2r+1} \end{bmatrix} = \begin{bmatrix} S_1 \\ S_2 \\ S_3 \\ S_4 \end{bmatrix}, \tag{26}$$

Boundary conditions are placed on separate matrices as follows:

$$\mathbf{A}_{11} = \begin{bmatrix} 1 & 0 & \cdots & 0 & 0 \\ \mathbf{D_{1,0}} & \mathbf{D_{1,1}} & \cdots & \mathbf{D_{1,M-1}} & \mathbf{D_{1,M}} \\ \hline & & A_{11} & & \\ \hline \mathbf{D_{M-1,0}} & \mathbf{D_{M-1,1}} & \cdots & \mathbf{D_{M-1,M-1}} & \mathbf{D_{M-1,M}} \\ 0 & 0 & \cdots & 0 & 1 \end{bmatrix}, \quad \mathbf{A}_{12} = \begin{bmatrix} 0 & 0 & \cdots & 0 & 0 \\ 0 & 0 & \cdots & 0 & 0 \\ \hline & & A_{12} & & \\ \hline 0 & 0 & \cdots & 0 & 0 \\ 0 & 0 & \cdots & 0 & 0 \end{bmatrix},$$

$$\mathbf{A}_{13} = \begin{bmatrix} 0 & 0 & \cdots & 0 & 0 \\ 0 & 0 & \cdots & 0 & 0 \\ \hline & & A_{13} & & \\ \hline 0 & 0 & \cdots & 0 & 0 \\ 0 & 0 & \cdots & 0 & 0 \end{bmatrix}, \quad \mathbf{A}_{14} = \begin{bmatrix} 0 & 0 & \cdots & 0 & 0 \\ 0 & 0 & \cdots & 0 & 0 \\ \hline & & A_{14} & & \\ \hline 0 & 0 & \cdots & 0 & 0 \\ 0 & 0 & \cdots & 0 & 0 \end{bmatrix}, \quad \mathbf{A}_{21} = \begin{bmatrix} 0 & 0 & \cdots & 0 & 0 \\ \hline & & A_{21} & & \\ \hline 0 & 0 & \cdots & 0 & 0 \end{bmatrix},$$

$$\mathbf{A}_{22} = \begin{bmatrix} 1 & 0 & \cdots & 0 & 0 \\ \hline & & A_{22} & & \\ \hline 0 & 0 & \cdots & 0 & 1 \end{bmatrix}, \quad \mathbf{A}_{23} = \begin{bmatrix} 0 & 0 & \cdots & 0 & 0 \\ \hline & & A_{23} & & \\ \hline 0 & 0 & \cdots & 0 & 0 \end{bmatrix}, \quad \mathbf{A}_{24} = \begin{bmatrix} 0 & 0 & \cdots & 0 & 0 \\ \hline & & A_{24} & & \\ \hline 0 & 0 & \cdots & 0 & 0 \end{bmatrix},$$

$$\mathbf{A}_{31} = \begin{bmatrix} 0 & 0 & \cdots & 0 & 0 \\ \hline & & A_{31} & & \\ \hline 0 & 0 & \cdots & 0 & 0 \end{bmatrix}, \quad \mathbf{A}_{32} = \begin{bmatrix} 0 & 0 & \cdots & 0 & 0 \\ \hline & & A_{32} & & \\ \hline 0 & 0 & \cdots & 0 & 0 \end{bmatrix}, \quad \mathbf{A}_{33} = \begin{bmatrix} 1 & 0 & \cdots & 0 & 0 \\ \hline & & A_{33} & & \\ \hline 0 & 0 & \cdots & 0 & 1 \end{bmatrix},$$

$$\mathbf{A}_{34} = \begin{bmatrix} 0 & 0 & \cdots & 0 & 0 \\ \hline & & A_{34} & & \\ \hline 0 & 0 & \cdots & 0 & 0 \end{bmatrix}, \quad \mathbf{A}_{41} = \begin{bmatrix} 0 & 0 & \cdots & 0 & 0 \\ \hline & & A_{41} & & \\ \hline 0 & 0 & \cdots & 0 & 0 \end{bmatrix}, \quad \mathbf{A}_{42} = \begin{bmatrix} 0 & 0 & \cdots & 0 & 0 \\ \hline & & A_{42} & & \\ \hline 0 & 0 & \cdots & 0 & 0 \end{bmatrix},$$

$$\mathbf{A_{43}} = \begin{bmatrix} 0 & 0 & \cdots & 0 & 0 \\ \hline & & A_{43} & & \\ \hline 0 & 0 & \cdots & 0 & 0 \end{bmatrix}, \quad \mathbf{A_{44}} = \begin{bmatrix} 1 & 0 & \cdots & 0 & 0 \\ \hline & & A_{44} & & \\ \hline 0 & 0 & \cdots & 0 & 1 \end{bmatrix}, \quad \mathbf{F}_{r+1} = \begin{bmatrix} f_{r+1,0} \\ f_{r+1,1} \\ \vdots \\ f_{r+1,M-1} \\ f_{r+1,M} \end{bmatrix},$$

$$\mathbf{G}_{r+1} = \begin{bmatrix} g_{r+1,0} \\ \vdots \\ g_{r+1,M} \end{bmatrix}, \quad \mathbf{\Theta_1}_{r+1} = \begin{bmatrix} \theta_{1r+1,0} \\ \vdots \\ \theta_{1r+1,M} \end{bmatrix}, \quad \mathbf{\Theta_2}_{r+1} = \begin{bmatrix} \theta_{2r+1,0} \\ \vdots \\ \theta_{2r+1,M} \end{bmatrix}, \quad S_1 = \begin{bmatrix} 1 \\ 0 \\ \mathbf{s_1} \\ 0 \\ -1 \end{bmatrix},$$

$$S_2 = \begin{bmatrix} 0 \\ \mathbf{s_2} \\ 0 \end{bmatrix}, \quad S_3 = \begin{bmatrix} 1 \\ \mathbf{s_3} \\ 0 \end{bmatrix}, \quad S_4 = \begin{bmatrix} 0 \\ \mathbf{s_4} \\ 0 \end{bmatrix}.$$

where

$$A_{11} = [\text{diag}(\mathbf{e}_{1,r}) \quad \text{diag}(\mathbf{e}_{2,r}) \quad \text{diag}(\mathbf{e}_{3,r}) \quad \text{diag}(\mathbf{e}_{4,r}) \quad \text{diag}(\mathbf{e}_{5,r})][\mathbf{D}^4 \quad \mathbf{D}^3 \quad \mathbf{D}^2 \quad \mathbf{D} \quad I]^T,$$

$$A_{12} = [\text{diag}(\mathbf{e}_{6,r})][\mathbf{D}^2]^T, \quad A_{13} = 0, \quad A_{14} = 0,$$

$$A_{21} = [1 \quad \text{diag}(\mathbf{e}_{7,r}) \quad \text{diag}(\mathbf{e}_{8,r})][D^2 \quad \mathbf{D} \quad I]^T,$$

$$A_{22} = [\text{diag}(\mathbf{e}_{9,r}) \quad \text{diag}(\mathbf{e}_{10,r}) \quad \text{diag}(\mathbf{e}_{11,r})][\mathbf{D}^2 \quad \mathbf{D} \quad I]^T, \quad A_{23} = 0,$$

$$A_{24} = 0, \quad A_{31} = [\text{diag}(\mathbf{e}_{12,r}) \quad \text{diag}(\mathbf{e}_{13,r})][D \quad I]^T, \quad A_{32} = [\text{diag}(\mathbf{e}_{13,r})][I]^T,$$

$$A_{33} = [\text{diag}(\mathbf{e}_{14,r}) \quad \text{diag}(\mathbf{e}_{15,r})][\mathbf{D}^2 \quad D]^T, \quad A_{34} = [\text{diag}(\mathbf{e}_{16,r})][I]^T,$$

$$A_{41} = [\text{diag}(\mathbf{e}_{17,r}) \quad \text{diag}(\mathbf{e}_{18,r}) \quad \text{diag}(\mathbf{e}_{19,r})][\mathbf{D}^2 \quad \mathbf{D} \quad I]^T,$$

$$A_{42} = [\text{diag}(\mathbf{e}_{20,r}) \quad \text{diag}(\mathbf{e}_{21,r})][\mathbf{D} \quad I]^T, \quad A_{43} = 0,$$

$$A_{44} = [1 \quad \text{diag}(\mathbf{e}_{22,r}), \quad \text{diag}(\mathbf{e}_{23,r})][D^2 \quad D \quad I].$$

Here, $\mathbf{e}$, $\mathbf{I}$, and $\mathbf{0}$ represent the diagonal, unit, and null matrices, respectively which are of order $(M + 1) \times (M + 1)$.
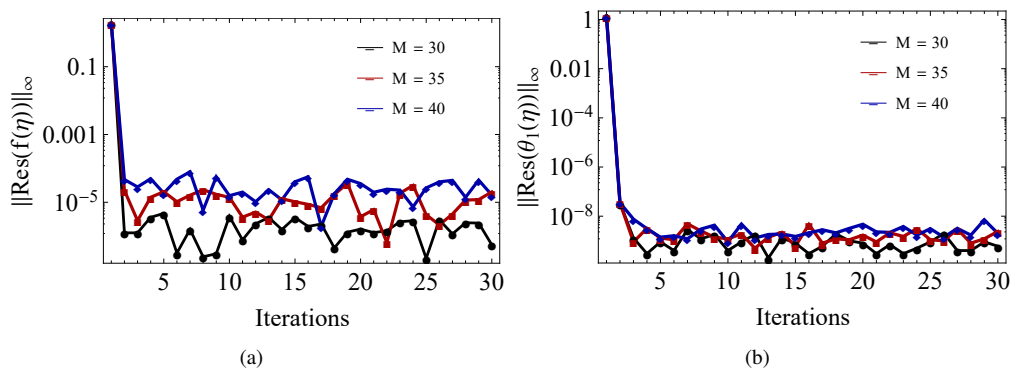

Figure 2. Influence of iterations on (a) $\|\text{Res}(f(\eta))\|_\infty$ and (b) $\|\text{Res}(\theta_1)\|_\infty$
for collocation points when $a_j = 1$, $m = 2$ $\phi = \pi/4$, $Re = 0.4$, $N = 0.4$, $Pr = 0.7$, $Br = 0.2$, $Da = 0.01$, $K = 0.5$.

4. CONVERGENCE ANALYSIS AND RESULTS

Convergence analysis entails demonstrating that the iterative procedure converges to an exact solution for the nonlinear differential equations (9) and (11), by taking the boundary conditions (13) into account. The calculation of residual errors is performed to guarantee the precision of the numerical results. Inaccuracies measure the extent of discrepancy between the numerical solution and the precise original solution. These errors quantify the degree of deviation experienced by the numerical solution from the original solution. For equations (9) and (11), the residual errors are obtained as follows:

$$\text{Res}(f) = \left(\frac{1}{1-N}\right)f^{iv} - \frac{N}{1-N}g'' + Re[f'f'' - ff'''] - \frac{1}{(1-N)Da}[K\cos^2\phi + \sin^2\phi]f'', \qquad (27)$$
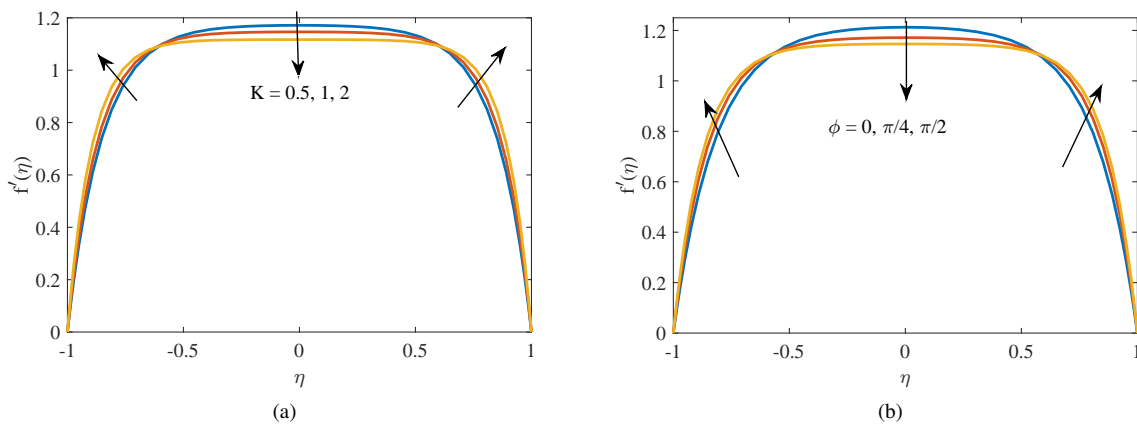
(a)

(b)

Figure 3. Axial velocity profile for different values of (a) Anisotropic permeability ratio K (b) Anisotropic angle ϕ for $aj = 1$, $m = 2$, $Re = 0.4$, $N = 0.4$, $Pr = 0.7$, $Br = 0.2$, $Da = 0.01$, $K = 0.5$, $\phi = \pi/4$.

$$\text{Res}(\theta_1) = \theta_1'' + 2\theta_2 - Pr\,Re\,[f\theta_1'] + \frac{N(2-N)}{1-N}\frac{Br}{m^2}g^2 + \frac{Br}{(1-N)Da}[\cos^2\phi + K\sin^2\phi]f^2 + 2\left(\frac{2-N}{1-N}\right)Brf'^2. \quad (28)$$

The infinite norms of (27) and (28) are represented as $\|\text{Res}(f)\|_\infty$, and $\|\text{Res}(\theta_1)\|_\infty$ respectively which indicate the largest absolute value of the error over the whole domain. Increasing the values of M(number of collocation points), affects the accuracy of the solution generated by SQLM, as illustrated in Figure (2). The residual error in f over 30 iterations for different collocation points ($M = 30, 35, 40$) is displayed in figure 2(a). The optimal accuracy is achieved with collocation points between 30 and 40, with residual errors around 10^{-6}. The residual error in θ_1 over 30 iterations is depicted in figure 2(b). Furthermore, the convergence becomes increasingly evident after the fifth iteration, as the residual error norms fall in between 10^{-9} to 10^{-10}. Effects of various key parameters on micropolar fluid flow and heat transfer characteristics are investigated. These parameters include Darcy number, Reynolds number, Prandtl number, Brinkman number, anisotropic ratio, anisotropic angle, and the coupling number.

Figures in (3) and (4), depict the axial velocity distribution $f'(\eta)$ against the dimensionless distance η. In figure 3(a),
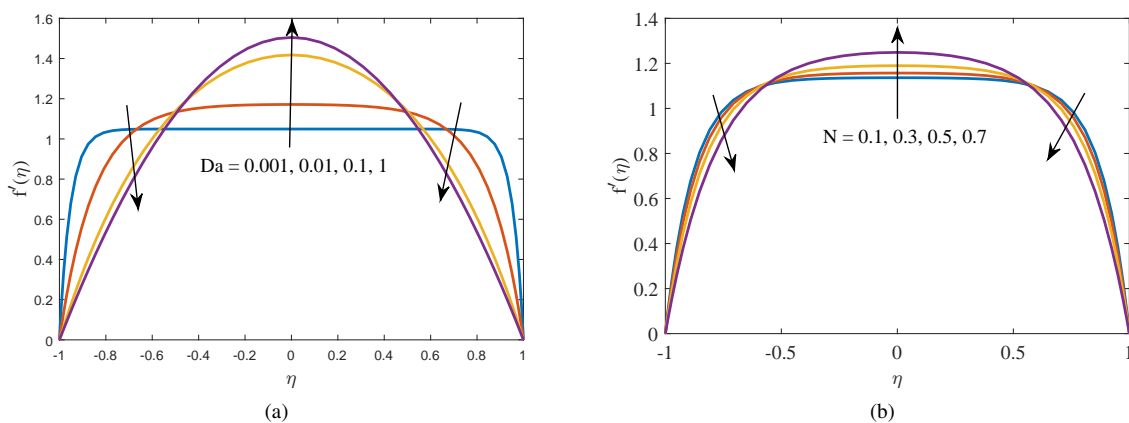

(a)

(b)

Figure 4. Axial velocity profile for different values of (a) Darcy number Da (b) Coupling number N for $aj = 1$, $m = 2$, $Re = 0.4$, $Pr = 0.7$, $Br = 0.2$, $Da = 0.01$, $K = 0.5$, $\phi = \pi/4$.

it is evident that the velocity rises near the vicinity of the boundaries as the values of permeability ratio K are increased. Whereas near the centre line, a decline can be noted, and maximum velocity is attained at the centre. This is due to the fact that the value of $k = k_1/k_2$ increases which implies the horizontal permeability decreases and so the velocity at the walls. Figure 3(b) depicts the variation of velocity with an anisotropic angle. Optimal velocity is attained when $\phi = 0$, while the lowest velocity is seen when $\phi = \frac{\pi}{2}$. This behaviour is consistent with the concept that when the value of K is less than or equal to 1 and keeps Da or k_1 constant, a value of $\phi = 0$ indicates a higher horizontal permeability k_2. Conversely, if the value of K is greater than 1, the behaviour will be the opposite. The value of $\phi = 0$ is equivalent to
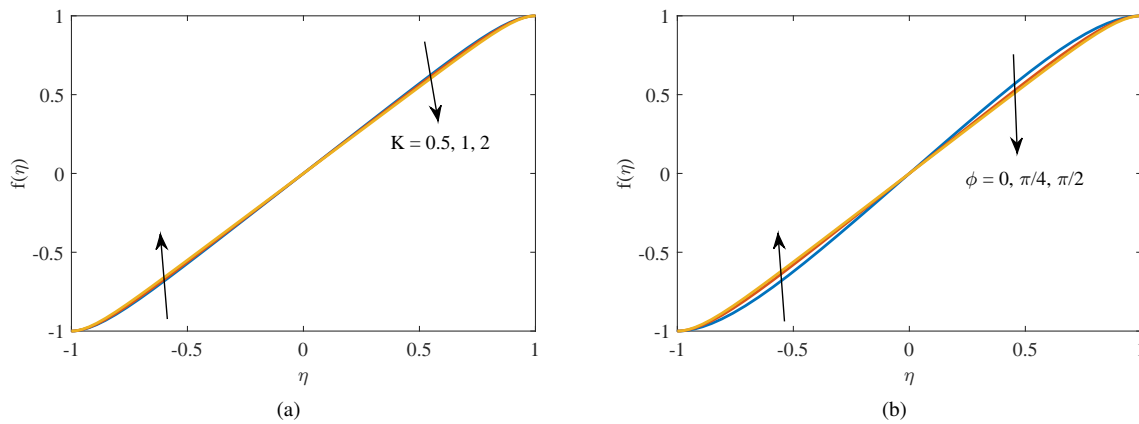
(a)

(b)

Figure 5. Transverse velocity profile for different values of (a) Anisotropic permeability ratio K (b) Anisotropic angle ϕ for $aj = 1$, $m = 3$, $Re = 0.2$, $N = 0.2$, $Pr = 0.7$, $Br = 0.2$, $Da = 0.01$, $K = 0.2$, $\phi = \pi/4$.

k_2 the horizontal permeability, resulting in a reduction in permeability along the flow direction. The velocity exhibits an upward trend in the vicinity of the walls and a downward trend at the centre as the angle increases. The graph in figure 4(a) illustrates a reduction in the velocity at boundaries and an increase at the centre of channel as the values of Da are raised. As Da increases from 0.001 to 1, the velocity profile shifts from uniform to parabolic, indicating less restricted fluid flow and increased velocity near the center. In the graph of figure 4(b), it can be observed that the velocity distribution is decreasing near the boundaries, whereas it is increasing at the centre. With increasing N, the influence of microrotations becomes more pronounced, leading to a flatter, more uniform velocity distribution across the channel. Figures (5)-(6), depict the transverse velocity profile $f(\eta)$ against the dimensionless distance η. Figure 5(a) illustrates that the transverse velocity rises at the lower boundary and reduces at the upper boundary, as the value of K is increased. Maximum velocity is attained at the upper wall. For a constant Da (constant k_1), an increase in K results in a decrease in k_2, the horizontal permeability. As k_2 diminishes, the shear resistance in the horizontal direction escalates, consequently enhancing the energy dissipation attributed to internal friction within the flow. This energy dissipation influences the overall decrease in fluid momentum and, indirectly, the transverse velocity as well. In figure 5(b), the velocity is seen rising near the lower boundary and decreasing towards upper boundary with an increase in ϕ. Elevating anisotropic angle ϕ causes the permeability of the porous media to align with the transverse direction. This alignment reduces resistance and induces redistributing of the fluid flow, so enhancing the transverse velocity component near the lower wall and a decrease at the upper wall. Figures in 6(a) and 6(b) show the effect of Da and N on the transverse velocity. The velocity
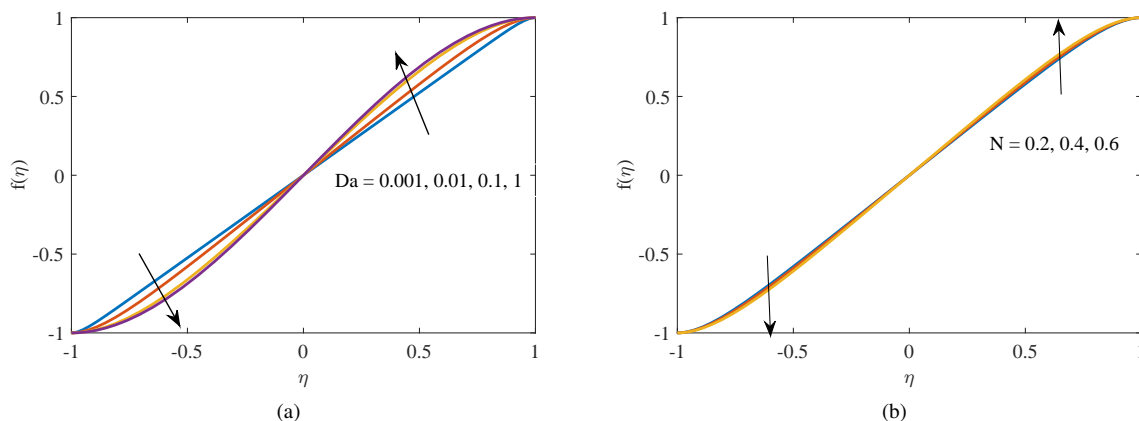

(a)

(b)

Figure 6. Transverse velocity profile for different values of (a) Darcy number Da (b) Coupling number N for $aj = 1$, $m = 3$, $Re = 0.2$, $N = 0.2$, $Pr = 0.7$, $Br = 0.2$, $Da = 0.01$, $K = 0.2$, $\phi = \pi/4$.

is observed to reduce near the lower boundary and rises from the centre towards the upper wall as values of Da and N are increased. This is expected because a higher Darcy number typically implies a more permeable medium, allowing fluid to move more freely. As N increases, the velocity profiles are almost overlapping with a slight shift upward. This

overlap suggests that variations in the coupling number have a relatively small impact on the transverse velocity. The
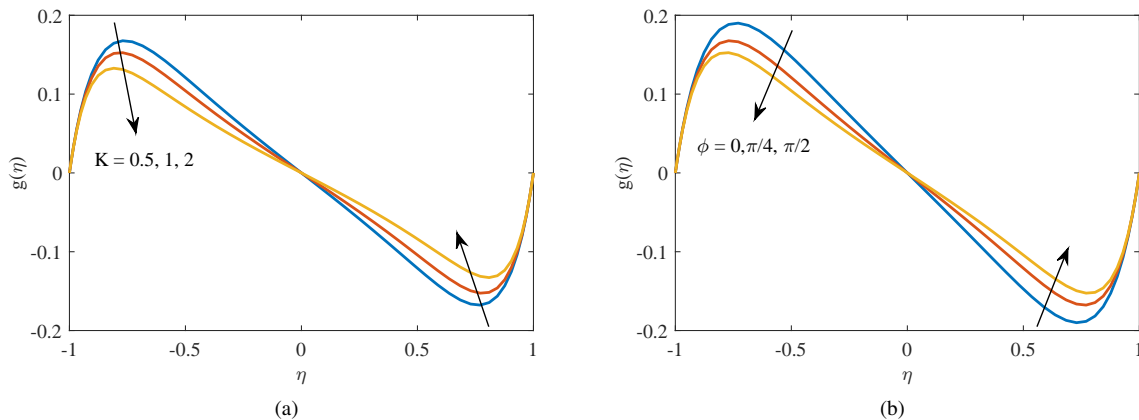

(a)

(b)

Figure 7. Microrotation profile for different values of (a) Anisotropic permeability ratio K (b) Aisotropic angle ϕ for $aj = 1$, $m = 2$, $Re = 0.2$, $N = 0.2$, $Pr = 0.7$, $Br = 0.2$, $Da = 0.01$, $K = 0.5$, $\phi = \pi/4$.

microrotation profile in figure 7(a) shows a wave-like pattern with distinct peaks and troughs. The amplitude of these oscillations, especially at the centre of the channel, can be seen to decrease. This is due to the dampening effects of rotation in the fluid as the anisotropic permeability K increases. Figure 7(b) demonstrates that increasing the anisotropic angle also reduces microrotation, affecting the rotational dynamics in the fluid. In figure 8(a), as Da increases, an increase in microrotation near the vicinity of lower wall is observed, which declines towards the upper wall. A higher Darcy number, corresponding to more permeable media, reduces microrotation effects. Understanding this relationship is crucial for accurately modelling fluid behaviour in micropolar systems, especially in industrial and biomedical applications where porous media play a significant role. Figure 8(b) demonstrates that increasing the values of coupling number N leads
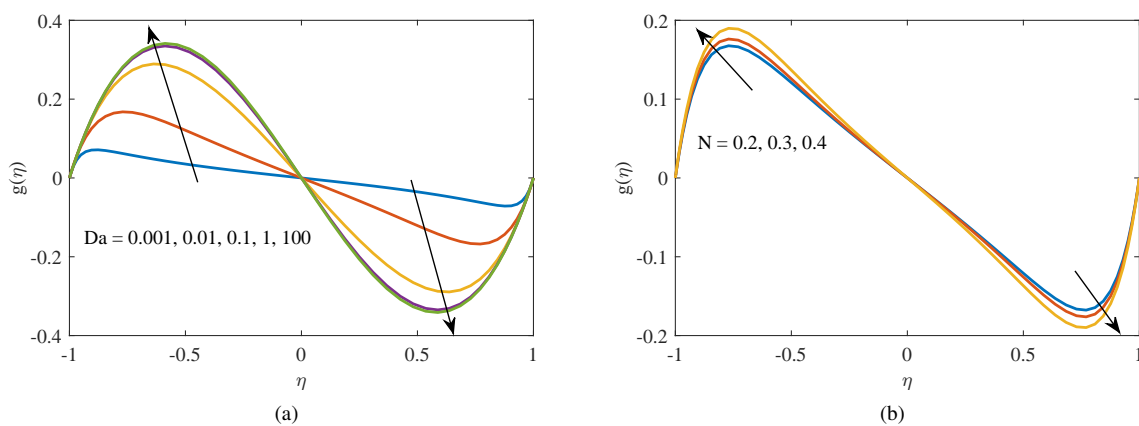

(a)

(b)

Figure 8. Microrotation profile for different values of (a) Darcy number Da (b) Coupling number N for $aj = 1$, $m = 2$, $Re = 0.2$, $N = 0.2$, $Pr = 0.7$, $Br = 0.2$, $Da = 0.01$, $K = 0.5$, $\phi = \pi/4$.

to reduction in microrotation located near the upper channel wall. This phenomenon occurs because an increase in the coupling number leads to a decrease in the thickness of the boundary layer. Furthermore, the microrotation is unimpeded by the microelements distributed over the metal plate. The microrotation profile in the boundary layer thickness is not hindered by the microelements that are dispersed away from the plate. Therefore, the distribution of microrotation is an increasing function of the coupling number till $\eta = 0$ and opposite from $\eta = 0$ to $\eta = 1$. Figures in (9) depict the reverse trend for increasing the values of Re, Pr, and Br. Figures in (10)- (12) depict the variation of temperature profile against the non-dimensional distance η. It can be seen from figure 10(a) the flatter curve is a result of increased permeability, which raises K values and results in a more uniform temperature distribution. Figure 10(b) shows that the temperature is decreasing when the anisotropic angle ϕ is increased. A wider and more uniform temperature distribution is indicated by the peak temperature's slight decrease with increasing anisotropic angle. According to this, better heat diffusion throughout
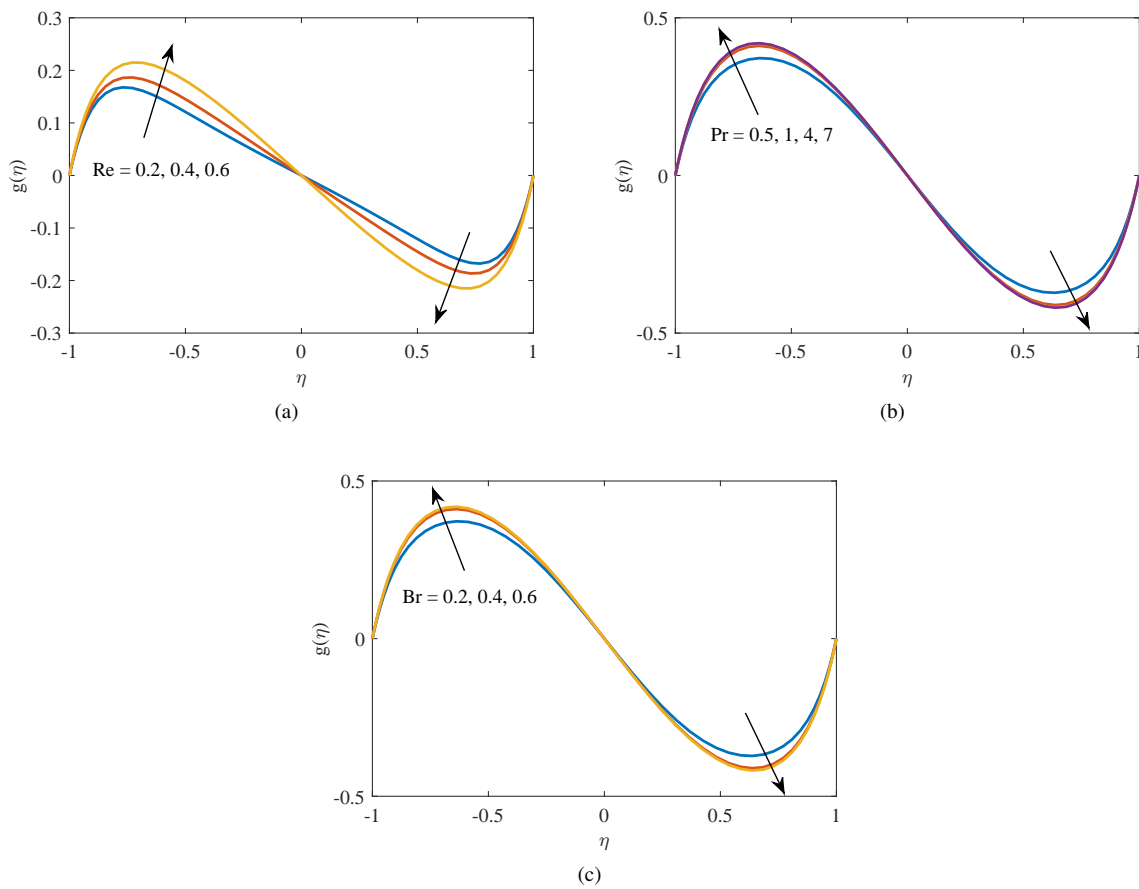
Figure 9. Microrotation profile for different values of (a) Reynold's number Re (b) Prandtl number Pr (c) Brinkman number Br, for $aj = 1$, $m = 2.4$, $Re = 0.75$, $N = 0.2$, $Pr = 0.7$, $Br = 0.2$, $Da = 0.01$, $K = 0.5$, $\phi = \pi/4$.
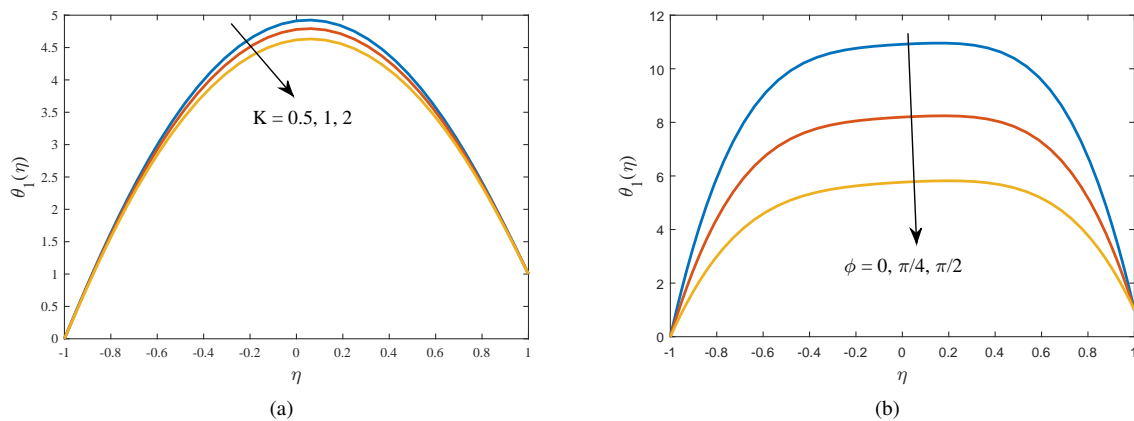

Figure 10. Temperature profile for different values of (a) Anisotropic permeability ratio K (b) Anisotropic angle ϕ for $aj = 1$, $m = 2$, $Re = 0.4$, $N = 0.4$, $Pr = 0.7$, $Br = 0.2$, $Da = 0.01$, $K = 0.5$, $\phi = \pi/4$.

the fluid is produced by larger anisotropic angles. The temperature reaches its maximum at the center of the wall and for $\phi = 0$. Figure 11(a) shows that higher Da values typically correspond to more permeable media, allowing for more efficient heat transfer. Figure 11(b) illustrates that higher values of N indicate more significant coupling effects, which enhance thermal diffusion, leading to a more uniform temperature profile. As Re increases, in figure 12(a), we observe that the temperature profile peaks near the center and reduces towards the boundaries. This indicates higher Reynold's
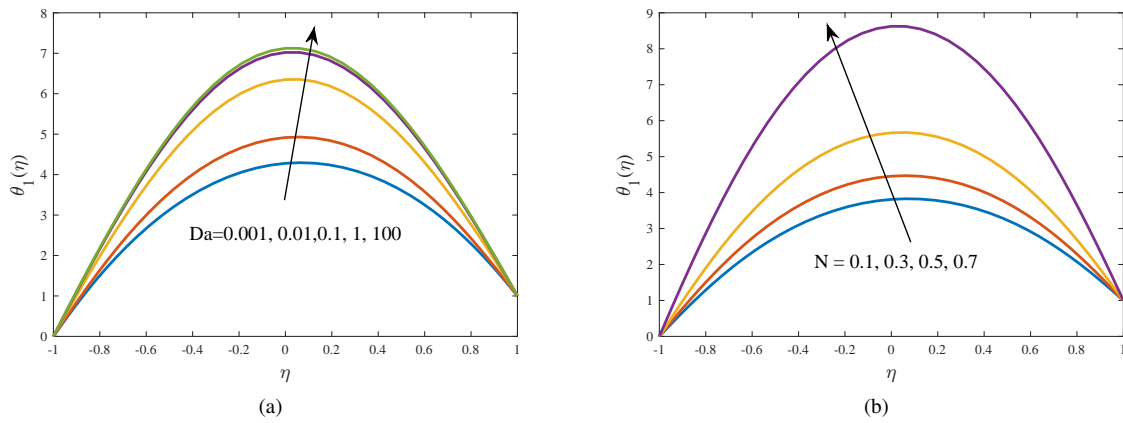
Figure 11. Temperature profile for different values of (a) Darcy number Da (b) Coupling number N for $aj = 1$, $m = 2$, $Re = 0.4$, $N = 0.4$, $Pr = 0.7$, $Br = 0.95$, $Da = 0.01$, $K = 0.5$, $\phi = \pi/4$.
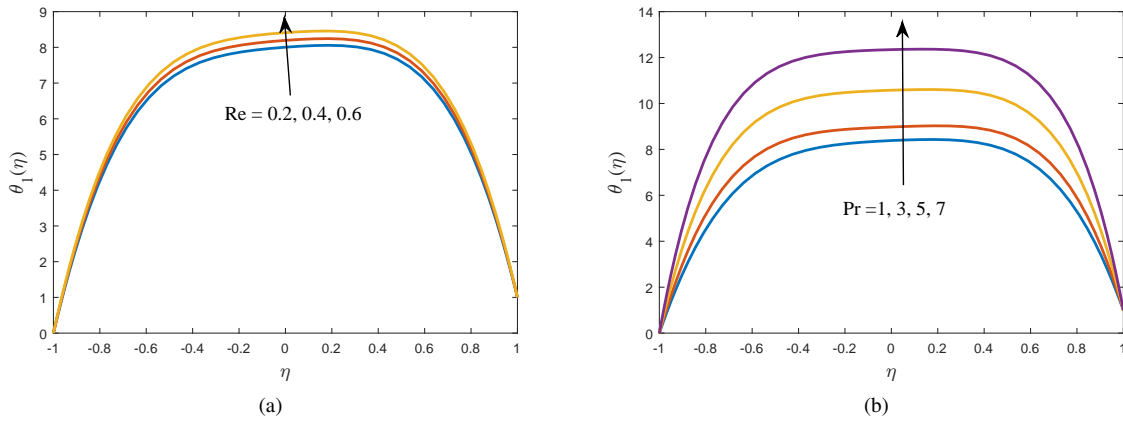

Figure 12. Temperature profile for different values of (a) Reynold's number Re (b) Prandtl number Pr for $aj = 1$, $m = 2$, $Re = 0.4$, $N = 0.4$, $Pr = 0.7$, $Br = 0.2$, $Da = 0.01$, $K = 0.5$, $\phi = \pi/4$.

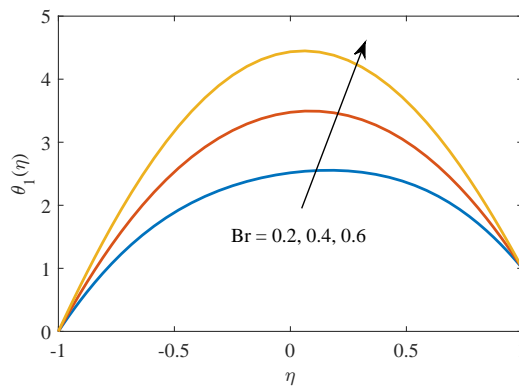**Figure 13.** Temperature profile for different values of Brikman number Br for $aj = 1$, $m = 2$, $Re = 0.4$, $N = 0.4$, $Pr = 0.7$, $Da = 0.1$, $K = 0.5$, $\phi = \pi/4$.

number leads to more uniform temperature distribution, resulting in enhanced heat transfer. Higher Re corresponds to higher flow rates or lower viscosity due to which the temperature gradient becomes less steep. Figure 12(b) illustrates

that the temperature peaks near $\eta = 0$ and decreases towards the boundaries as the value of Pr increases. Greater Prandtl number Pr values result in decreased thermal diffusion and more pronounced temperature gradients, which results in more localised changes near the center. Figure (13) shows that increasing the value of Brinkman number Br, results in a higher temperature peak, indicating that viscous dissipation effects become more significant.

5. CONCLUSIONS

The present work introduces a mathematical model that describes the dynamics of fluid flow and the heat transfer of a micropolar fluid within a conduit that is saturated with anisotropic porous media. The numerical solutions are obtained using a Spectral Quasi-Linearization Method (SQLM). An in-house developed MATLAB program is used to generate graphs that depict the impacts of some important physical parameters identified in the review. The results obtained are summarized as follows:

- Anisotropic permeability ratio and angle significantly impact the fluid flow and heat characteristics. As K, ϕ increases, the microrotation and temperature increase, whereas the velocity reduces at the centre of the wall, and rises near the end of the walls.

- Higher values of Darcy number (Da) indicate less restricted flow, leading to decreased axial velocity near the walls and increased transverse velocity at the upper wall due to higher vertical permeability. This also reduces microrotation effects. Understanding this relationship is essential for accurately modelling fluid behavior in micropolar systems, particularly in industrial and biomedical applications involving porous media. Additionally, the temperature tends to rise near the centre of the channel.

- Increasing coupling number N leads to a reduction in velocity and microrotation in conjunction with an increase in temperature, mostly due to the substantial micropolar effects.

- As the Brinkmann number Br increases, the viscous dissipation effects cause microrotation at the upper channel wall and temperature to decrease.

- Increase in Reynolds number Re, causes the microrotation to decrease after the middle of channel and the temperature distribution becomes less pronounced, indicating stronger convective effects.

- Higher Prandtl number Pr leads to reduced microrotation and increased temperature, indicating improved heat transfer efficiency attributed to increased thermal conductivity.

The convergence analysis demonstrated that the SQLM is effective. The residual errors for velocity and temperature profiles showed rapid convergence, with accuracy significantly improving after the fifth iteration. Accuracy reached its peak at 35-40 collocation points, but then gradually declined. The numerical method proved robust and efficient, with residual error norms ranging from 10^{-6} to 10^{-7} and 10^{-9} to 10^{-10} for various parameters.

The present work addresses a research gap by investigating the impact of micropolar fluid dynamics on fluid flow and heat transfer. The paper offers valuable recommendations for enhancing the transfer of heat and flow control in engineering applications that involve micropolar fluids. The numerical method is found to be robust and efficient.

ORCID
R. Vijaya Sree, https://orcid.org/0009-0002-0047-302X; V. K. Narla, https://orcid.org/0000-0003-0994-3497

REFERENCES
[1] A.C. Eringen, "Theory of micropolar fluids," J. Math. Mech. **16**, 1–18 (1966). https://doi.org/10.1512/iumj.1967.16.16001

[2] R.S.R. Gorla, and A.S. Kumari, "Buoyancy effects on the boundary layer flow of a micropolar fluid along a vertical cylinder," Int. J. Eng. Sci. **26**(8), 883–892 (1988). https://doi.org/10.1016/0020-7225(88)90039-0

[3] R.S.R. Gorla, R. Pender, and J. Eppich, "Heat transfer in micropolar boundary layer flow over a flat plate," Int. J. Eng. Sci. **21**(7), 791–798 (1983). https://doi.org/10.1016/0020-7225(83)90062-9

[4] R.S.R. Gorla, "Mixed convection in a micropolar fluid from a vertical surface with uniform heat flux," Int. J. Eng. Sci. **30**(3), 349–358 (1992). https://doi.org/10.1016/0020-7225(92)90080-Z

[5] A. Arafa, and R.S.R. Gorla, "Mixed convection boundary layer flow of a micropolar fluid along vertical cylinders and needles," Int. J. Eng. Sci. **30**(12), 1745–1751 (1992). https://doi.org/10.1615/InterJFluidMechRes.v33.i3.10

[6] D.D. Ganji, and A. Mirzaaghaian, "Application of differential transformation method in micropolar fluid flow and heat transfer through permeable walls," Alex. Eng. J. **55**, 2183–2191 (2016). https://doi.org/10.1016/j.aej.2016.06.011

[7] J.K. Zhou, *Differential Transformation and its Applications for Electrical Circuits*, (Huazhong University Press, Wuhan, 1986).

[8] D.D. Ganji, and A.S. Dogonchi, "Analytical investigation of convective heat transfer of a longitudinal fin with temperature-dependent thermal conductivity, heat transfer coefficient and heat generation," Int. J. Phys. Sci. **9**(21), 466–474 (2014). https://academicjournals.org/journal/IJPS/article-full-text-pdf/417CC2548549

[9] A.S. Dogonchi, M. Hatami, and D.D. Ganji, "Motion analysis of a spherical solid particle in plane Couette Newtonian fluid flow," Powder Technol. **274**, (2015). https://doi.org/10.1016/j.powtec.2015.01.018

[10] A.S. Dogonchi, M. Hatami, Kh. Hosseinzadeh, and G. Domairry, "Non-spherical particles sedimentation in an incompressible Newtonian medium by Pade approximation," Powder Technol. **278**, 248–256 (2015). https://doi.org/10.1016/j.powtec.2015.03.036

[11] A.S. Dogonchi and D.D. Ganji, "Convection–radiation heat transfer study of moving fin with temperature-dependent thermal conductivity, heat transfer coefficient and heat generation," Appl. Therm. Eng. **103**, 705–712 (2016). https://doi.org/10.1016/j.applthermaleng.2016.04.121

[12] F. Mabood, S.M. Ibrahim, M.M. Rashidi, M.S. Shadloo, and G. Lorenzini, "Non-uniform heat source/sink and Soret effects on MHD non-Darcian convective flow past a stretching sheet in a micropolar fluid with radiation," Int. J. Heat Mass Transf. **93**, 674–682 (2016). https://doi.org/10.1016/j.ijheatmasstransfer.2015.10.014

[13] M. Fakour, A. Vahabzadeh, D.D. Ganji, and M. Hatami, "Analytical study of micropolar fluid flow and heat transfer in a channel with permeable walls," J. Mol. Liq. **204**, 198–204 (2015). https://doi.org/10.1016/j.molliq.2015.01.040

[14] N. Sandeep and C. Sulochana, "Dual solutions for unsteady mixed convection flow of MHD micropolar fluid over a stretching/shrinking sheet with non-uniform heat source/sink," Eng. Sci. Technol. Int. J. **18**(4), 738–745 (2015). https://doi.org/10.1016/j.jestch.2015.05.006

[15] M. Turkyilmazoglu, "Mixed convection flow of magnetohydrodynamic micropolar fluid due to a porous heated/cooled deformable plate: Exact solutions," Int. J. Heat Mass Transf. **106**, 127–134 (2017). https://doi.org/10.1016/j.ijheatmasstransfer.2016.10.056

[16] M. Turkyilmazoglu, "Flow of a micropolar fluid due to a porous stretching sheet and heat transfer," Int. J. Non-Linear Mech. **83**, 59–64 (2016). https://doi.org/10.1016/j.ijnonlinmec.2016.04.004

[17] P.P. Humane, V.S. Patil, A.B. Patil, and M.D. Shamshuddin, "Buongiorno modelled nanoliquid consequence of thermal and solutal convection on the magneto-micropolar fluid inside an inclined porous stretching device," J. Nanofluids, **12**(1), 211–222 (2023). https://doi.org/10.1166/jon.2023.1949

[18] V. Agarwal, B. Singh, A. Kumari, W. Jamshed, K.S. Nisar, A.H. Almaliki, and H.Y. Zahran, "Steady Magnetohydrodynamic Micropolar Fluid Flow and Heat and Mass Transfer in Permeable Channel with Thermal Radiation," Coatings, **12**(1), 11 (2021). https://doi.org/10.3390/coatings12010011

[19] B. Jalili, A.A. Azar, P. Jalili, and D.D. Ganji, "Analytical approach for micropolar fluid flow in a channel with porous walls," Alexandria Eng. J. **79**, 196–226 (2023). https://doi.org/10.1016/j.aej.2023.08.015

[20] M. D. Shamshuddin, F. Mabood, W.A. Khan, and G.R. Rajput, "Exploration of thermal Peclet number, vortex viscosity, and Reynolds number on two-dimensional flow of micropolar fluid through a channel due to mixed convection," Heat Transf. **52**(1), 854–873 (2023). https://doi.org/10.1002/htj.22719

[21] M. Abdalbagi, "Micropolar flow and heat transfer within a permeable channel using the successive linearization method," Open Physics, **21**(1), (2023). https://doi.org/10.1515/phys-2023-0177

[22] Z. Shah, A. Khan, W. Khan, M.K. Alam, S. Islam, P. Kumam, and P. Thounthong, "Micropolar gold blood nanofluid flow and radiative heat transfer between permeable channels," Comput. Methods Programs Biomed. **186**, 105197 (2020). https://doi.org/10.1016/j.cmpb.2019.105197

[23] S. Ahmad, M. Ashraf, K. Ali, and K.S. Nisar, "Computational analysis of heat and mass transfer in a micropolar fluid flow through a porous medium between permeable channel walls," Int. J. Nonlinear Sci. Numer. Simul. **23**(5), 761–775 (2022). https://doi.org/10.1515/ijnsns-2020-0017

[24] M. Akbarzadeh, S. Rashidi, M. Bovand, and R. Ellahi, "A sensitivity analysis on thermal and pumping power for the flow of nanofluid inside a wavy channel," J. Mol. Liq. **220**, 1–13 (2016). https://doi.org/10.1016/j.molliq.2016.04.058

[25] M.M. Bhatti, M.M. Rashidi, "Effects of thermo-diffusion and thermal radiation on Williamson nanofluid over a porous shrinking/stretching sheet," J. Mol. Liq. **221**, 567–573 (2016). https://doi.org/10.1016/j.molliq.2016.05.049

[26] M.M. Rashidi, N. Vishnu Ganesh, A.K. Abdul Hakeem, B. Ganga, , "Buoyancy effect on MHD flow of nanofluid over a stretching sheet in the presence of thermal radiation," J. Mol. Liq. **198**, 234–238 (2014). https://doi.org/10.1016/j.molliq.2014.06.037

[27] H.S. Takhar, R. Bhargava, R.S. Agrawal, and A.V.S. Balaji, "Finite element solution of micropolar fluid flow and heat transfer between two porous discs," Int. J. Eng. Sci. **38**(17), 1907–1922 (2000). https://doi.org/10.1016/S0020-7225(00)00019-7

[28] M. Pathak, P. Joshi, and K.S. Nisar, "Numerical investigation of fluid flow and heat transfer in micropolar fluids over a stretching domain," J. Therm. Anal. Calorim. **147**, 10637–10646 (2022). https://doi.org/10.1007/s10973-022-11268-w

[29] C. Boodoo, "Micropolar fluid flows past a porous shell: A model for drug delivery using porous microspheres," Eur. J. Eng. Technol. Res. **9**(3), 1–7 (2024). https://doi.org/10.24018/ejeng.2024.9.3.3162

[30] D. Srinivasacharya and K. Hima Bindu, "Entropy generation in a porous annulus due to micropolar fluid flow with slip and convective boundary conditions," Energy, **111**, 165–177 (2016). https://doi.org/10.1016/j.energy.2016.05.101

[31] R.A. Alharbey, H. Mondal, and R. Behl, "Spectral quasi-linearization method for non-Darcy porous medium with convective boundary condition," Entropy, **21**(9), 838 (2019). https://doi.org/10.3390/e21090838

[32] T. Karmakar, M. Reza, and G.P.R. Sekhar, "Forced convection in a fluid saturated anisotropic porous channel with isoflux boundaries," Physics of Fluids, **31**, 117109 (2019). https://doi.org/10.1063/1.5126892

[33] I.P. Grant, R.E. Bellman, and R.E. Kalaba, "Quasilinearization and Non-Linear Boundary Value Problems," Math. Gaz. **52**(380), 212 (1968). https://doi.org/10.2307/3612757

[34] C. Canuto, M.Y. Hussaini, A. Quarteroni, and T.A. Zang, *Spectral Methods*, Vol. 285, (Springer, 2006).

[35] D. Srinivasacharya, and K.H. Bindu, "Entropy generation in a micropolar fluid flow through an inclined channel with slip and convective boundary conditions," Energy, **91**(C), 72–83 (2015). https://doi.org/10.1016/j.energy.2016.05.101

ВПЛИВ АНІЗОТРОПНОЇ ПРОНИКНОСТІ НА МІКРОПОЛЯРНУ ДИНАМІКУ РІДИНИ ТА ТЕПЛОПЕРЕНОС У ПОРИСТИХ КАНАЛАХ

Р. Віджая срі[a,b], **В. К. Нарла**[b]

[a]Інженерний коледж АСЕ, Гхаткесар Мандал, округ Медчал, Телангана, 501301, Індія
[b]GITAM, факультет математики, Хайдарабад, 502329, Індія

У поточному дослідженні вивчається динаміка рідин та характеристики теплопередачі мікрополярних рідин у каналі, заповненому анізотропним пористим середовищем. Керівні рівняння для профілів потоку рідини, мікрообертання та температури розв'язуються чисельно за допомогою методу спектральної квазілінеаризації (SQLM). Дослідження вивчає вплив різних ключових параметрів, таких як коефіцієнт анізотропної проникності, анізотропний кут, число Дарсі, число Рейнольдса, число Брінкмана, число Прандтля та число зв'язку. Ключові висновки вказують на те, що коефіцієнт анізотропної проникності та анізотропний кут значно впливають на потік рідини та розподіл тепла, при цьому підвищена анізотропія призводить до посиленого мікрообертання та температури, хоча й зі зниженою швидкістю в центрі каналу. Вищі числа Дарсі призводять до менш обмеженого потоку, збільшення швидкості та зменшення ефектів мікрообертання, тоді як збільшення числа сполучення сприяє більш рівномірному температурному профілю. Ці результати дають суттєве уявлення про оптимізацію теплопередачі та керування потоком у інженерних додатках, які включають мікрополярні рідини в пористих середовищах. Ключові слова: мікрополярні рідини, анізотропні пористі середовища, анізотропна проникність, мікроротація, теплопередача, метод спектрально-квазілінеаризації.

Ключові слова: *мікрополярна рідина; анізотропні пористі середовища; анізотропна проникність; мікроротація; теплообмін; спектральний квазілінеаризаційний метод*